This article has been accepted for publication in a future issue of this journal, but has not been fully edited. Content may change prior to final publication. Citation information: DOI 10.1109/ACCESS.2018.2806228, IEEE Access

Random Walker Framework for Sensor-based Echocardiography Fusion

Abhilash R. Hareendranathan, Michelle Noga, Pierre Boulanger, Harald Becher, and Kumaradevan Punithakumar, *Senior Member, IEEE,*

***Abstract*—Image fusion techniques in 3D echocardiography attempt to improve the field-of-view by combining multiple 3D ultrasound (3DUS) volumes. Echocardiography fusion techniques are mostly based on either image registration or sensor tracking. Compared to registration techniques, sensor tracking approaches are image independent and do not need any spatial overlap between the images. Once the images are spatially aligned the pixel intensities in the overlapping regions are determined using fusion algorithms such as average fusion (AVG) and maximum fusion (MAX). However, averaging generally results in reduced contrast while maximizing results in amplification of noise artifacts in the fused image. Wavelet fusion (WAV) overcomes these issues by selectively enhancing the low-frequency components in the image, but this could result in pixelation artifacts. We propose a new method for image fusion based on a generalized random walker framework (GRW) using ultrasound confidence maps. The maps are based on: 1) focal properties of the transducer; and 2) second order image features. The fusion technique was validated on image pairs sampled from 3DUS volumes acquired from 6 healthy volunteers. All the images were spatially aligned using optical tracking, and the fusion algorithm was used to determine the pixel intensity in the overlapping region.Comparisons based on quantitative measures showed statistically significant improvements for GRW ($\mathbf{p < 0.01}$) when compared to AVG, MAX, and WAV for Contrast to Noise Ratio (CNR): $\mathbf{0.85 \pm 0.03}$, Signal to Noise Ratio (SNR): $\mathbf{7.42 \pm 1.98}$, Wang-Bovik metric (Q0): $\mathbf{0.80 \pm 0.15}$. The Piella metric (Q1): $\mathbf{0.82 \pm 0.01}$ also gave higher values for GRW, but the difference was not statistically significant. Upon visual inspection, the GRW fusion had the lowest amount of stitching and pixelation artifacts. The fusion technique proposed could help in improving the diagnostic accuracy and clinical acceptance of 3D echocardiography.**

***Index Terms*—3D Echocardiography, Multiview fusion, Random Walker, Ultrasound Confidence Maps, Optical tracking**

I. Introduction

Three-dimensional (3D) echocardiography provides accurate, high-quality visualization of the heart and is commonly used for volumetric measurements such as the left ventricular (LV) ejection fraction [1]. Relative advantages of 3D echocardiography compared to 2DUS are well established [1]–[4] especially for volumetric analysis of aneurysms [2], [3] where 2D model based approaches usually are less accurate. 3D echocardiography also offers benefits in terms of operational cost and equipment complexity when compared to cardiac magnetic resonance (CMR) imaging.

A major limitation of 3D echocardiography is its limited field-of-view (FOV) which is caused due to limitations in physical dimensions of the transducer and lack of an ideal sonographic window. These limitations can reduce the clinical applicability of 3D echocardiography as it deprives the clinician of a complete 3D view of the heart. Consequently, attempts to fuse multiple cardiac images obtained at different scanning angles have received considerable research interest. Image fusion approaches in echocardiography are mostly based on either image registration [5]–[10] or sensor tracking [11]–[14].

Echocardiography volumetric data can be fused using image registration provided there is sufficient overlap between the constituent images. However clinical images of the heart such as the apical and parasternal views that contain complementary information are spatially far apart. In such cases, the requirement of substantial image overlap limits the extent of FOV improvement. Sensor-tracking based fusion techniques [11]–[14] overcome this limitation by tracking the ultrasound probe in 3D space and using this information for spatial alignment. Tracking based approaches also have the additional advantage of being independent of image resolution.

Once the images are spatially aligned, the next step is to determine the image intensity of the fused image in overlapping regions. The intuitive approach of averaging the pixel intensities would result in poor contrast (as image boundaries get blurred in the composite image). On the other hand using the maximum intensity has the disadvantage of the maximizing noise artifacts (such as speckle noise). Multiscale decomposition (MSD) techniques using wavelets have been proposed to overcome the issues mentioned above. Rajpoot et al. [7] extended 3D wavelet-based fusion to echocardiography images. In their work images from multiple views were initially registered using a rigid registration technique and then decomposed into multiple-frequency sub-bands. Then the low-frequency components were maximized, and high-frequency components were averaged. This ensured high-frequency noise suppression while preserving the speckled nature of the image. Punithakumar et al. [12] proposed a likelihood estimator based approach for wavelet fusion wherein each pixel was weighted based on the local image intensity in the neighborhood. Variants of the wavelet-transforms such as contourlets [15], curvelets [16], complex wavelets [17], [18] and beamlets [19] have also been proposed. One limitation of transform

A. R. Hareendranathan, M. Noga, P. Boulanger, and K. Punithakumar are with Department of Radiology & Diagnostic Imaging, University of Alberta, AB, Canada, and also with Servier Virtual Cardiac Centre, Mazankowski Alberta Heart Institute, AB, Canada

P. Boulanger and K. Punithakumar are also with Department of Computing Science, University of Alberta, AB, Canada.

H. Becher is with the ABACUS Center, Mazankowski Alberta Heart Institute, Edmonton, AB, Canada.

Corresponding author: A. R. Hareendranathan (hareendr@ualberta.ca)

This article has been accepted for publication in a future issue of this journal, but has not been fully edited. Content may change prior to final publication. Citation information: DOI 10.1109/ACCESS.2018.2806228, IEEE Access

based techniques (such as wavelets) is the presence pixelation artifacts which might distort small details in the fused image. Pixelation occurs due to decimations involved in the wavelet transform and translation dependence of standard wavelets [20]. As an alternative, variational approaches such as [21] have been proposed. These approaches are based on optimizing an energy-functional and usually involve continuous optimization which is computationally expensive. Computational cost and time can be considerably reduced by using discrete optimizations techniques such as graphs cuts which are very popular in image segmentation, smoothing and stereo vision. Miles et al. [20] used Graph cuts to fuse computed tomography (CT) and magnetic resonance (MR) images of the spine. They formulated image fusion as a multi-label optimization problem using alpha expansion. Discrete optimization can also be done using random walker (RW) formulations [22], [23] which offer two advantages: 1) it reduces the chance of small cuts for labels with a small boundary cost; and 2) it provides a confidence rating of each pixel's membership in the segmentation. A generalized RW formulation was proposed by Shen et al. [24] for fusing multi-exposure camera images. To the best of our knowledge, discrete optimization techniques have not been used for echocardiographic images to date. In this paper, we propose a generalized RW formulation (GRW) for multi-view ultrasound image fusion using ultrasound confidence maps (UCM). UCMs have been used to provide pixel confidence estimates for applications such as shadow detection, 3D freehand ultrasound reconstruction and multimodal image registration [25]. The probability map proposed in this paper is different from Karamalis et al. as we 1) define pixel probability as inverse weights for floating nodes based on distance from the focal point of ultrasound transducer, and 2) we use second-order image features to estimate the presence of tubular structures such myocardial boundaries and leaflets based on the filter developed by Frangi et al. [26].

II. Methodology

An overview of the proposed image fusion technique is shown in Figure 1. As shown in the figure, we align the individual ultrasound volumes based on the positional information obtained from the optical tracking system.The position and orientation of the ultrasound probe were tracked using an Optitrack (NaturalPoint, Corvallis, OR, USA) optical tracking system which had sub-millimeter precision. Our method allows six degree of freedom (6 DOF) which captures translational and rotational components. As an initial calibration the position of the ultrasound probe w.r.t a global coordinate system was obtained by scanning the probe using a laser scanner (Kreon Technologies, Limoges, France), which was calibrated to an expected accuracy of 57 μm. The spatial transformations required to align the image were computed using the approach mentioned in Punithakumar *et al.* [12]. Upon obtaining spatially aligned images, we formulate image fusion as an RW optimization problem and introduce pixel-wise information as a UCM. The UCM assigns higher confidence values to pixels that are closer to ultrasound focus and closer to transducer axis. The confidence values are also increased based on the presence of second order (ridge-like) features. The formulations for the GRW and UCMs are described below.

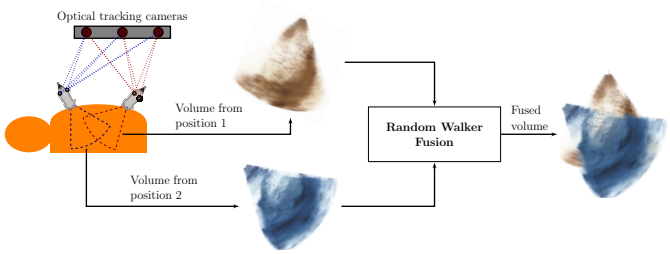

Fig. 1. Schematic representation of the proposed echocardiography fusion system using optical tracking system for spatial alignment and generalized random walker for final image intensity computation.

A. Ultrasound Confidence Maps (UCM)

The UCM gives a pixel-wise likelihood estimate ranging from 0 to 1 based on the location and neighbourhood information of the pixel. We define UCM, U_i, as follows:

$$U_i = (d_{f,i} + d_{a,i}) \exp(-\alpha d_{o,i}) \exp(-\beta F_i) \tag{1}$$

where d represents the distance of point i from the focal point f , nearest point to the axis of the transducer a and geometric center of the transducer array o. These are defined using a L^2-norm such that:

$$\begin{aligned} d_{f,i} &= \|i - f\|^2 \\ d_{a,i} &= \|i - a\|^2 \\ d_{o,i} &= \|i - o\|^2 \end{aligned} \tag{2}$$

F_i is a vesselness function computed based on eigen value decomposition [26]. Using eigen values (λ_1, λ_2) of the Hessian matrix H we define F_i as:

$$F_i = \begin{cases} 0 & \text{if } \lambda_2 > 0 \\ 1 - \exp\left(\frac{\lambda_1}{\lambda_2}\right) + \exp(\lambda_1 + \lambda_2) & \text{if } \lambda_2 < 0 \end{cases} \tag{3}$$

The Hessian matrix H is computed as the convolution of the image I over the second order derivatives of a Gaussian filter bank G which can be written as:

$$G(x, s) = \frac{1}{2\pi} s^2 \exp\left(-\frac{\|x\|^2}{2s^2}\right) \tag{4}$$

The term s represents the scale of the Gaussian filter, and it was empirically set to 2. Similarly, the two free parameters, α and β, were empirically chosen for the entire dataset.

B. Generalized Random Walker Formulation for Multiview Image Fusion

The RW approach formulates fusion as a multi-labeling problem. For a set of n images coming from multiple views $M = \{I_1, \ldots, I_n\}$ and set of labels $L = \{l_1, \ldots, l_n\}$ corresponding to these views, RW algorithm finds the probability p of each pixel in the fused image having a label $l \in L$. Note

This article has been accepted for publication in a future issue of this journal, but has not been fully edited. Content may change prior to final publication. Citation information: DOI 10.1109/ACCESS.2018.2806228, IEEE Access

that we assume the images to be either registered or aligned by tracking such that there is a one-to-one correspondence between the pixel intensities in each image. The pixel intensity in the fused image g_i^f can be calculated as the average of the pixel intensities from the individual views g_i^k weighted by their probability p_i^k.

$$g_i^f = \frac{1}{n}\sum_{k=1}^{n} g_i \times p_i^k \tag{5}$$

The set of pixels in fused image F and corresponding labels L are represented by nodes on an undirected graph $G = (V, E)$ where $V = (F \cup L)$ and $E = F \times L$. The RW formulation finds the probability that a random walker starting from an image node $V_f \in F$ reaches a particular label node $V_l \in L$. The weights for the image edges and label edges are represented by ω_{ij} defined as:

$$\omega_{ij} = \begin{cases} \exp\left(-(g_i - g_j)\right) & \forall j \in F \\ \exp\left(-(l - U_i)\right) & \forall j \in L \end{cases} \tag{6}$$

where U_i is the pixel probability of pixel obtained from the UCM. A schematic representation of a node in the GRW formulation is shown in Figure 2.

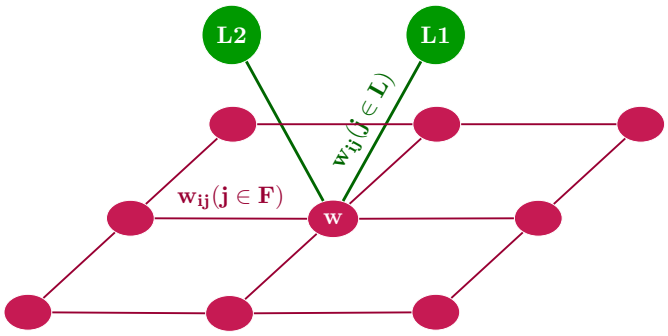

Fig. 2. Schematic representation of diagonally connected neighbourhood of a node in the GRW formulation.

Based on the equivalence of RW formulation and electrical networks described by Grady [23], we denote the node potential of $v_i \in V$ as $u(v_i)$. The total energy of the network can then be described in terms of a quadratic functional of the edge weights as:

$$E = \frac{1}{2}\sum_{(v_i, v_j)} \omega_{ij}\left(u(v_i) - u(v_j)\right)^2 \tag{7}$$

Grady [23] has shown that any harmonic function can minimize the energy functional in (7). This harmonic function can be efficiently computed using the Laplacian matrix $\mathcal{L}$ which represents the edge weights as:

$$\mathcal{L}_{ij} = \begin{cases} d_i & \text{if } i = j \\ \omega_{ij} & \text{if } (i,j) \in V \\ 0 & \text{otherwise} \end{cases} \tag{8}$$

The Laplacian matrix $\mathcal{L}$ can be rearranged using upper triangular matrices $\mathcal{L}_L$, $\mathcal{L}_X$ and $\mathcal{R}$ as:

$$\mathcal{L} = \begin{bmatrix} \mathcal{L}_L & \mathcal{R} \\ \mathcal{R}^T & \mathcal{L}_X \end{bmatrix} \tag{9}$$

As shown by Shen et al. [24], the solution to the combinatorial Dirichlet problem in (7) can be solved by rewriting (7) in matrix form as :

$$E = \begin{pmatrix} u_L \\ u_X \end{pmatrix}^T \begin{bmatrix} \mathcal{L}_L & \mathcal{R} \\ \mathcal{R}^T & \mathcal{L}_X \end{bmatrix} \begin{pmatrix} u_L \\ u_X \end{pmatrix} \tag{10}$$

where $u_L = (u(l_1)...u(l_k))$ represents the label nodes and $u_x = (u(x_1)...u(x_N))$ represents the image nodes.The minimum energy solution of (7) can be obtained by setting $\nabla E = 0$ in equation (10) and solving for :

$$\mathcal{L}_X u_X = -\mathcal{R}^T u_L \tag{11}$$

The estimated contribution p_i^k of an individual view k for a pixel location i can be found by solving k such combinatorial formulations.

The ultrasound image acquisition setup and quantitative metrics used for evaluation are explained next.

C. Data Acquisition

In this study, we acquired 18 three-dimensional ultrasound (3DUS) volume pairs of echocardiography data from 6 healthy volunteers. All sequences were acquired on a Philips iE33 ultrasound scanner (Philips Healthcare, Best, The Netherlands) using an X3-1 matrix array transducer. The protocol was approved by the Health Research Ethics Board of the University of Alberta, and informed consent was obtained from all volunteers. Volume rates were varied from 7 to 34 per cardiac cycle. Each 3DUS volume constituted of $176 \times 176 \times 208$ pixels with resolutions in the range of $(74 \times 74 \times 63)$ to (85×85) mm in x, y, and z coordinate directions, respectively. During scanning, the ECG from the ultrasound scanner was transmitted and read using an NI USB-6009 digitizer. We also developed a software module to detect the R-wave using LabVIEW so as to ensure that volumes correspond to similar points in the cardiac cycle. A test data set of 60 2D images was randomly sampled from the 3D volumes for quantitative evaluation.

D. Metrics for Quantitative evaluation of Image Fusion

In this study, we compared four fusion techniques - average fusion (AVG), maximum fusion (MAX), wavelet fusion (WVL) and GRW fusion - using quantitative metrics. We used four metrics for comparison - signal to noise ratio (SNR), contrast to noise ratio (CNR), Wang-Bovik metric (Q0) [27] and Piella metric (Q1) [28]. These metrics are calculated as follows:

$$SNR = \frac{\mu_{MY}}{\mu_{BP}} \tag{12}$$

$$CNR = \frac{(\mu_{MY} - \mu_{BP})}{\mu_{BP}} \tag{13}$$

The subscripts MY and BP refer to myocardial and blood pool regions selected around the contours as shown in Figure

This article has been accepted for publication in a future issue of this journal, but has not been fully edited. Content may change prior to final publication. Citation information: DOI 10.1109/ACCESS.2018.2806228, IEEE Access

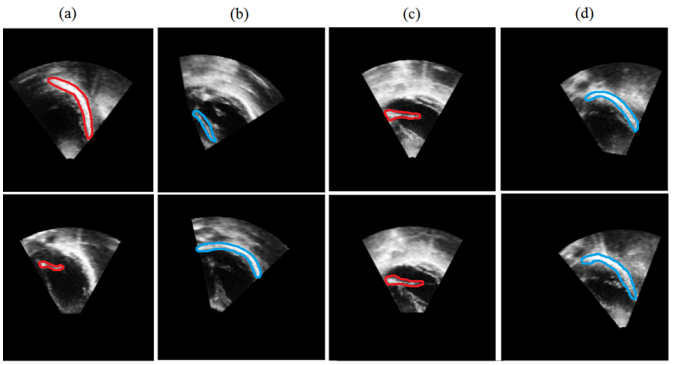

Fig. 3. A few examples of manual segmentation on individual slices delineating the myocardial boundary and leaflets. Corresponding views are shown pairwise in figures (a) and (b), and figures (c) and (d).

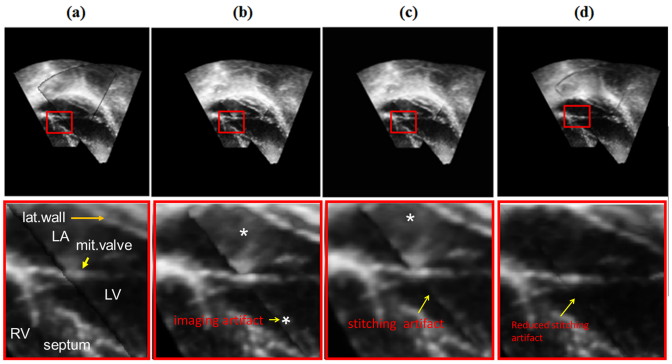

Fig. 4. First row: Fused image slice from various fusion techniques (a) AVG (b) MAX (c) WAV and (d) the proposed GRW, second row: Magnified view showing the left-ventricle (LV), right-ventricle (RV), mitral valve, septum and lateral-wall of the heart. Note the imaging artifacts shown by the asterisk (*) in row 2b and c are considerably reduced in GRW fusion.

3. The terms μ and σ^2 represent the mean and variance of pixel intensities in the region.

In order to quantify the amount of features retained in the fused image, we computed the Wang-Bovik metric (Q0) and Piella metric (Q1). To calculate the Wang-Bovik metric, a reference image R was chosen from the individual views v_1 and v_2 based on the segmentation masks. Given a reference image R and fused image F the Wang-Bovik metric can be calculated as:

$$\mathrm{Q0} = \frac{4\sigma_{RF}\mu_R\mu_F}{(\mu_R^2+\mu_F^2)(\sigma_R^2+\sigma_F^2)} \tag{14}$$

For the Piella metric Q1, we define a saliency feature $\eta(w)$ over a window w based on the ratio of mean to standard deviation:

$$\eta(w) = \frac{\mu_1/\sigma_1^2}{(\mu_1/\sigma_1^2)+(\mu_2/\sigma_2^2)} \tag{15}$$

Then, the Piella metric can be calculated as:

$$\mathrm{Q0}(v_1,v_2,F) = \frac{1}{\|W\|}\sum_{w\in W}\Big(\eta(w)\mathrm{Q0}(v_1,F) + (1-\eta(w))\mathrm{Q1}(v_2,F)\Big) \tag{16}$$

III. Results

The images obtained in this study were spatially aligned using optical tracking. The GRW fusion algorithm was implemented in Matlab version 8.6 (R2015b). The execution time for the algorithm was less than 10 seconds per ultrasound image while running on a 3.2 GHz CPU. We manually segmented the myocardial boundary and leaflets, examples of which are shown in Figure 1. The SNR and CNR were calculated by comparing the pixel intensities inside the mask to pixel intensities in the immediate neighborhood. A reference image Iref was created using the segmentation masks (shown in Figure 3) which was then used to compute the Wang-Bovik metric Q0. Similarly to compute the Piella metric Q1 we defined a saliency feature based on the signal-to-noise ratio inside the segmentation masks. An example of the image fusion is shown in Figure 4. The GRW fusion gave significantly higher values for all four indices, and it did not have pixelation artifacts in the fused image since the approach does not involve transformation (as shown in row 2 of Figure 4). GRW fusion also considerably reduced the stitching which can be clearly seen in other fusion techniques.

The quantitative indices - CNR, SNR, Q0, and Q1 for a dataset of 60 images fused using each of the techniques is compared in Table I. GRW gave higher values for all indices calculated. The differences for all matrices were statistically significant (at $p < 0.01$) when analyzed using a paired t-test for CNR, SNR, and Q0.

The color map shows high probability pixels in blue and low probability in red. As shown in Figure 5, pixels corresponding to the cardiac structures were assigned to a higher probability (dark blue) in the UCM. The impact of the free parameters α and β on the ultrasound confidence map was also studied. As shown in Figure 5, increasing the α value resulted in shrinking the focal region (shown in blue). Similarly, when the β value was increased, small echogenic structures were assigned to higher probabilities in UCMs resulting in a grainy pattern. As shown in Figure 5 optimal performance was obtained for $\alpha = 1$ and $\beta = 2$.

IV. Discussion

In order to optimize the image quality of fused echocardiography datasets, we proposed a GRW formulation using UCMs. Senor based fusion is a two-step process involving 1) spatial alignment of images and 2) finding the optimal image intensity of each pixel location in the fused image. The spatial alignment determined using sensor position is independent of image-overlap and image quality. In non-overlapping regions of the fused image the image intensity from the single view is retained. The proposed GRW formulation determines the optimal pixel intensity in overlapping regions of the fused image, and it was tested with datasets from volunteers for the first time. Main advantages of the proposed technique, when compared to existing techniques, are that it accounts for pixel neighborhood intensities and ultrasound transducer characteristics (via the UCM).

This article has been accepted for publication in a future issue of this journal, but has not been fully edited. Content may change prior to final publication. Citation information: DOI 10.1109/ACCESS.2018.2806228, IEEE Access

TABLE I
COMPARISON OF QUANTITATIVE INDICES FOR VARIOUS FUSION METHODOLOGIES, VALUES ARE REPRESENTED AS MEAN ± STANDARD DEVIATION. GRW FUSION YIELDED THE BEST VALUE FOR ALL QUANTITATIVE MEASURES.

Fusion Method	**CNR**	**SNR**	**Q0**	**Q1**
Average (AVG)	0.84 ± 0.04	7.11 ± 2.0	0.60 ± 0.1	0.72 ± 0.12
Maximum (MAX)	0.83 ± 0.04	6.96 ± 1.90	0.53 ± 0.14	0.80 ± 0.12
Wavelet (WAV)	0.84 ± 0.03	7.16 ± 1.94	0.70 ± 0.13	0.78 ± 0.14
Generalized Random Walker (GRW)	$\mathbf{0.85 \pm 0.03}$	$\mathbf{7.42 \pm 1.98}$	$\mathbf{0.80 \pm 0.15}$	$\mathbf{0.82 \pm 0.12}$

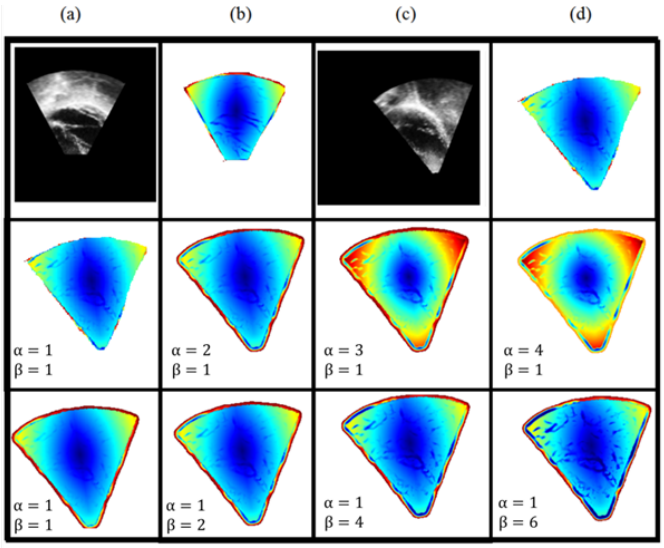

Fig. 5. Examples of slices from the fused image volume shown row-wise, first row: (a), (b) individual views of heart and corresponding probability maps (c), (d), Effect of free parameters on the UCM is illustrated in rows 2-3, which show variation of and respectively.

The performance of the proposed fusion technique was evaluated using CNR, SNR, Wang-Bovik metric (Q0) and Piella metric (Q1). While CNR and SNR indicated image quality, Q0 and Q1 indicated the amount of relevant information preserved in the fused image. Compared to other commonly used fusion techniques such as AVG, MAX, and WAV, the GRW gave higher values for all four quality indices: CNR, SNR, Q0 and Q1. Also as demonstrated in Figure 3 the fusion technique does not result in pixelation artifacts since the approach does not involve transformation. We also observed only a small number of stitching artifacts in the GRW fusion when compared to AVG fusion where the effects of stitching were apparent.

The proposed provides an ideal framework to seamlessly integrate the various transducer characteristics such as focusing as well as image features into the fusion algorithm. The UCM provided a confidence estimate for each pixel in the fused image, and these probabilities were used as label-edge weights. As this formulation leaves the lattice structure of the RW formulation intact, we could use the optimization schemes mentioned by Grady [23]. Since cardiac structures such as leaflets and the myocardial boundaries are seen as echogenic tubular structures, the UCM assigned higher probabilities to these structures.

Fusion methods have been proposed to overcome some of the major hurdles which limit the more extensive use of 3D echo: the limited FOV and the limited image quality in many patients. Over the last years, progress has been made to develop techniques to accurately align 3D datasets obtained from different positions on the chest. Recently our group has reported a technique using optical tracking which was used in this study to obviate the need for image overlap between individual views and is also independent of image resolution. This is beneficial in echocardiography as the ultrasound image volumes usually have high levels of speckle noise. We were also able to fuse image volumes obtained at large angular separation such as parasternal and apical views of the heart which usually contain complementary information [13]. The generalized random walker framework (GRW) using ultrasound confidence maps (UCM) is another step towards a clinically applicable 3D echocardiography fusion method.

The ultrasound scanning takes $\approx$ 5 seconds per volume for a 4–beat acquisition but varies with the patients anatomy. During the study, parasternal and apical views were acquired within single breath-holds (within 10 to 15 seconds) as well as multiple breath-holds (15 to 20 seconds). The optical tracking runs simultaneously and does not introduce any additional delay. The post-processing time was $\approx$ 10 seconds per image. However, in order to fuse an entire cardiac cycle (with $\approx$30 frames), the algorithm might take a more significant amount of time in which case GPU computation techniques would have to be developed. In this study, we used data sets with large variations in volume rate (7 to 34 per cardiac cycle). The low volume rates correspond to single breath-holds and the higher volume rates correspond to multiple breath-holds. We did not notice any difference in the quality of fusion in both cases which illustrates the robustness of the approach. Usually low-volume-rate data sets are not used for clinical measurements (such as ejection fraction) due to poor temporal resolution.

Although the fusion technique has been tested for cardiac images, it could be extended to other organs like the carotid artery, aorta, and 3-D fetal femur. Further, there are no limitations on the number of views that can be fused. However, we found that two spatially-apart views were sufficient to cover the entire LV boundary.

One limitation of our study is that it was conducted on a small number of subjects all of which were healthy volunteers with relatively good acoustic windows. We have only acquired still frames at breath-hold and effect of free breathing has not been examined. An extension of this study to a more

substantial number of subjects including patients with heart disease is planned as a future work. Note that in this case, the advantage of the FOV improvement could be more apparent.

On the technical aspect of limitations, the optical tracking is restricted to line-of-sight [12]. During the experiment we determined the optimal position of multi-camera system inside the scanning room so as to minimize the line-of-sight issue. In a separate study, we have examined the feasibility of magnetic tracking on dynamic heart phantom [14], and in future, we plan to test the magnetic tracking on healthy volunteers. One of the limitations of all the fusion techniques described (including ours) is that fast moving structures such as valves could be duplicated in the fused image. Our future work would aim to extend the proposed RW formulation to 3D so that we could fuse complete 3D volumes instead of individual slices thereby accounting for pixel information in the all three dimensions. By extending the RW formulation to 3D we would also be able to fuse full loops of ultrasound images which would be beneficial in visualizing moving structures.

V. Conclusion

A new approach for echocardiography image fusion based on generalized random walker formulation was introduced in this paper. The new method was able to incorporate transducer characteristics and image features into the fusion and showed higher values for various image quality metrics than other commonly used fusion approaches. The fusion technique also reduced pixelation or stitching artifacts. We expect that this technique could add substantial value to diagnostic echocardiography and we suggest further studies in patients.

VI. Acknowledgment

We acknowledge Servier Canada Inc., Collaborative Health Research Projects (CHRP) and Heart & Stroke Foundation of Alberta, NWT and Nunavut for the research grants that supported this work. A. R. Hareendranathan was partly funded by a research grant from Radiological Society of North America (RSNA). The GPU used in this research for rendering was donated by the NVIDIA Corporation.

References

[1] V. Mor-Avi, L. Sugeng, and R. M. Lang, "Real-time 3-dimensional echocardiography: An integral component of the routine echocardiographic examination in adult patients?" *Circulation*, vol. 119, no. 2, pp. 314–329, 2009.

[2] C. Jenkins, K. Bricknell, L. Hanekom, and T. H. Marwick, "Reproducibility and accuracy of echocardiographic measurements of left ventricular parameters using real-time three-dimensional echocardiography," *Journal of the American College of Cardiology*, vol. 44, no. 4, pp. 878–886, 2004.

[3] C. Jenkins, J. Chan, L. Hanekom, and T. H. Marwick, "Accuracy and feasibility of online 3-dimensional echocardiography for measurement of left ventricular parameters," *Journal of the American Society of Echocardiography*, vol. 19, no. 9, pp. 1119 – 1128, 2006.

[4] R. M. Lang, V. Mor-Avi, L. Sugeng, P. S. Nieman, and D. J. Sahn, "Three-dimensional echocardiography: The benefits of the additional dimension," *Journal of the American College of Cardiology*, vol. 48, no. 10, pp. 2053–2069, 2006.

[5] Y. Ma, K. Rhode, G. Gao, A. King, P. Chinchapatnam, T. Schaeffter, D. Hawkes, R. Razavi, and G. Penney, "Ultrasound calibration using intensity-based image registration: for application in cardiac catheterization procedures," in *Medical Imaging*. International Society for Optics and Photonics, 2008, pp. 69 180O–69 180O.

[6] C. Yao, J. M. Simpson, T. Schaeffter, and G. P. Penney, "Multi-view 3D echocardiography compounding based on feature consistency," *Physics in Medicine and Biology*, vol. 56, no. 18, p. 6109, 2011.

[7] K. Rajpoot, V. Grau, J. A. Noble, H. Becher, and C. Szmigielski, "The evaluation of single-view and multi-view fusion 3D echocardiography using image-driven segmentation and tracking," *Medical Image Analysis*, vol. 15, no. 4, pp. 514–528, 2011.

[8] A. Nasim, A. G. Hafeez, K. Rajpoot, and M. S. Younis, "Investigating 3D echocardiography image fusion for improving image quality," in *3rd International Conference on Computer, Control & Communication*. IEEE, 2013, pp. 1–6.

[9] G. Piella, M. D. Craene, C. Butakoff, V. Grau, C. Yao, S. Nedjati-Gilani, G. P. Penney, and A. F. Frangi, "Multiview diffeomorphic registration: application to motion and strain estimation from 3D echocardiography," *Medical Image Analysis*, 2013.

[10] D. Augustine, M. Yaqub, C. Szmigielski, E. Lima, S. E. Petersen, H. Becher, J. A. Noble, and P. Leeson, ""3D fusion" echocardiography improves 3D left ventricular assessment: Comparison with 2D contrast echocardiography," *Echocardiography*, vol. 32, no. 2, pp. 302–309, 2015.

[11] K. Punithakumar, P. W. Wood, M. Biamonte, M. Noga, P. Boulanger, and H. Becher, "Cardiac ultrasound multiview fusion using a multi-camera tracking system," in *IEEE-EMBS International Conference on Biomedical and Health Informatics (BHI)*, 2014, pp. 318–321.

[12] K. Punithakumar, A. R. Hareendranathan, A. McNulty, M. Biamonte, A. He, M. Noga, P. Boulanger, and H. Becher, "Multiview 3-D echocardiography fusion with breath-hold position tracking using an optical tracking system," *Ultrasound in Medicine & Biology*, vol. 42, no. 8, pp. 1998 – 2009, 2016.

[13] A. R. Hareendranathan, K. Punithakumar, M. A. Hanbidge, W. He, M. Noga, P. Boulanger, and H. Becher, "Patient movement compensation for 3D echocardiography fusion," in *The 38th Annual International Conference of the IEEE Engineering in Medicine and Biology Society*, Aug 2016, pp. 1091–1094.

[14] K. Punithakumar, A. R. Hareendranathan, R. Paakkanen, N. Khan, M. Noga, P. Boulanger, and H. Becher, "Multiview echocardiography fusion using an electromagnetic tracking system," in *The 38th Annual International Conference of the IEEE Engineering in Medicine and Biology Society*, Aug 2016, pp. 1078–1081.

[15] Y. Zheng, Y. Wu, and H. Zhang, "Image fusion using a hybrid representation of empirical mode decomposition and contourlet transform," in *International Conference on Information Science and Technology*, March 2011, pp. 577–582.

[16] F. Nencini, A. Garzelli, S. Baronti, and L. Alparone, "Remote sensing image fusion using the curvelet transform," *Information Fusion*, vol. 8, no. 2, pp. 143 – 156, 2007.

[17] P. Hill, N. Canagarajah, and D. Bull, "Image fusion using complex wavelets," in *Proceedings of the British Machine Vision Conference*. BMVA Press, 2002, pp. 47.1–47.10.

[18] J. J. Lewis, R. J. OCallaghan, S. G. Nikolov, D. R. Bull, and N. Canagarajah, "Pixel- and region-based image fusion with complex wavelets," *Information Fusion*, vol. 8, no. 2, pp. 119 – 130, 2007.

[19] G. M. Zhang and Z. M. Cui, "A novel image fusion method using beamlet transform and graph cuts," in *Materials, Mechatronics and Automation*, ser. Key Engineering Materials, vol. 467. Trans Tech Publications, 5 2011, pp. 1092–1096.

[20] B. Miles, I. B. Ayed, M. W. K. Law, G. Garvin, A. Fenster, and S. Li, "Spine image fusion via graph cuts," *IEEE Transactions on Biomedical Engineering*, vol. 60, no. 7, pp. 1841–1850, July 2013.

[21] G. Piella, "Image fusion for enhanced visualization: Avariationalapproach," *International Journal of Computer Vision*, vol. 83, no. 1, pp. 1–11, Jun 2009.

[22] L. Grady, "Multilabel random walker image segmentation using prior models," in *2005 IEEE Computer Society Conference on Computer Vision and Pattern Recognition (CVPR'05)*, vol. 1, June 2005, pp. 763–770 vol. 1.

[23] ——, "Random walks for image segmentation," *IEEE Transactions on Pattern Analysis and Machine Intelligence*, vol. 28, no. 11, pp. 1768–1783, Nov 2006.

[24] R. Shen, I. Cheng, J. Shi, and A. Basu, "Generalized random walks for fusion of multi-exposure images," *IEEE Transactions on Image Processing*, vol. 20, no. 12, pp. 3634–3646, Dec 2011.

[25] A. Karamalis, W. Wein, T. Klein, and N. Navab, "Ultrasound confidence maps using random walks," *Medical Image Analysis*, vol. 16, no. 6, pp. 1101 – 1112, 2012.

[26] A. F. Frangi, W. J. Niessen, K. L. Vincken, and M. A. Viergever, "Multiscale vessel enhancement filtering." Springer-Verlag, 1998, pp. 130–137.
[27] Z. Wang and A. C. Bovik, "A universal image quality index," *IEEE Signal Processing Letters*, vol. 9, no. 3, pp. 81–84, March 2002.
[28] G. Piella and H. Heijmans, "A new quality metric for image fusion," in *Proceedings 2003 International Conference on Image Processing (Cat. No.03CH37429)*, vol. 3, Sept 2003, pp. III–173–6 vol.2.